Geomechanics and Engineering, *Vol. 25, No. 6 (2021) 535-552*
DOI: https://doi.org/10.12989/gae.2021.25.6.535

Crack development and coalescence process in drying clayey loess

Xin Wei[1a], Mahdia Hattab[2b], Said Taibi[3c], Katia V. Bicalho[4d], Ling Xu[*1] and Jean-Marie Fleureau[5e]

[1]School of Human Settlement and Civil Engineering, Xi'an Jiaotong University,
28 Xianning Road, 700054 Xi'an, Shaanxi Province, People's Republic of China
[2]Laboratory of Microstructures and Mechanics of Materials, University of Lorraine,
CNRS UMR 7239, Arts et Métiers ParisTech, 57000 Metz, France
[3]Laboratory of Waves and Complex Media, University of Havre,
CNRS UMR 6294, 25 rue Philippe Lebon, 76600 Le Havre, France
[4]Department of Civil Engineering, Federal University of Espirito Santo,
Av. Fernando Ferrari, 514 - Goiabeiras, Vitória - ES, Brasil, 29075-910
[5]Laboratory of Mechanics of Soils, Structures and Materials, Paris-Saclay University, Centrale Supélec
CNRS UMR 8579, 3 rue Joliot Curie, 91190 Gif sur Yvette, France

(Received September 1, 2020, Revised May 28, 2021, Accepted June 16, 2021)

Abstract. The Chinese Loess Plateau is located in northwestern China. During investigations in loess fields, it was found that, under dry climatic conditions, cracks were prone to appear and propagate in the loess plateau. The presence of cracks and their effect on the engineering properties of loess greatly influence the stability of soil-based structures and can cause severe damages. The purpose of this research was to analyze the drying-induced cracking mechanisms in clayey loess, and to highlight the effect of soil mineralogy. Laboratory tests were performed to simulate the cracking process in loess. The analysis is based on the local two-dimensional strain and displacement fields derived from the Digital Image Correlation (DIC) method and the software VIC-2D. The determination of the mechanical strain tensors, i.e., the difference between the total strain and shrinkage strain tensors, and their visual representation allow a deeper understanding of cracking mechanisms. Based on the above methods, crack development and crack coalescence processes were observed and analyzed. Besides, other mechanisms were identified, such as junction and bifurcation of cracks.

Keywords: clayey loess; digital image correlation; crack development; mechanical strain tensors; coalescence; bifurcation; junction processes

1. Introduction

Loess exists in many parts of the world, especially in arid and semi-arid climate areas. The Chinese Loess Plateau approximately covers 440,000 km^2 in northwestern China in the upper and middle reaches of the Yellow River. Loess is a special geo-material that features randomly distributed heterogeneities, such as microcracks, pores, cracks and joints. Microcracks and cracks tend to appear on the ground surface of the loess plateau. Each crack alters the in-situ stress state in the cracked area, influencing the soil behavior as well as the deformation of the cracked area. The presence of cracks and their effect on the engineering properties of loess are of fundamental interest in various geotechnical, water management, and environmental applications (Wang 2000, Lu *et al.* 2005, Sun 2007).

More generally, the evolution of cracks in clayey soils can significantly alter soil hydro-mechanical behavior, weaken soil performance, create preferential paths for the rain water in slopes and accelerate surface erosion (Baker 1981, Lee *et al.* 1988, Silvestri *et al.* 1992, Tay *et al.* 2001, Li *et al.* 2011, Tang *et al.* 2011, Li *et al.* 2016). The variation of the hydraulic and mechanical properties (e.g., tensile strength) of a soil is closely related to its hydric state, i.e., its suction. At the scale of the continuous medium, it is generally accepted that cracks occur when tensile and shear stresses caused by shrinkage exceed the strength of the soil. In other cases, due for example to boundary conditions, non-uniform drying, or inclusion presence, complex patterns of shear stresses set up. Practical measurements of tensile strength of clayey soils have been reported by a few researchers, e.g. Avila (2004) on slurry soils, Tang *et al.* (2010) and Li *et al.* (2019) on compacted soils. Avila (2004) presented the results of direct measurements of the tensile strength of clay with double triangular-shaped specimens, for samples prepared at different initial suctions. Fracture mechanics was applied to analyze the initiation and evolution of cracks in clayey soils

∗Corresponding author, Professor
E-mail: xuling82@xjtu.edu.cn
[a]Associate Professor
E-mail: weixinstar@xjtu.edu.cn
[b]Professor
E-mail: mahdia.hattab@univ-lorraine.fr
[c]Professor
E-mail: said.taibi@univ-lehavre.fr
[d]Professor
E-mail: katia.bicalho@ufes.br
[e]Professor
E-mail: jean-marie.fleureau@centralesupelec.fr

ISSN: 2005-307X (Print), 2092-6219 (Online)

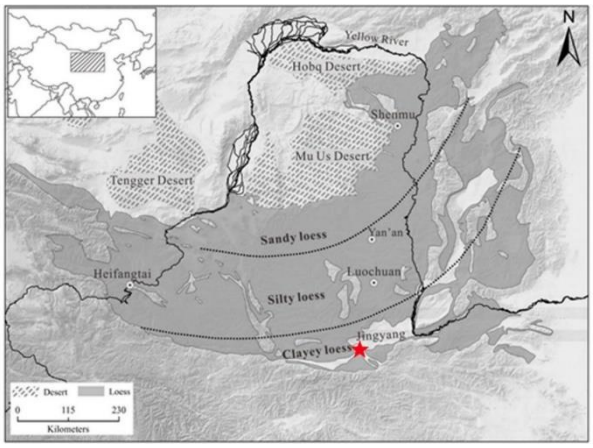

Fig. 1 Location of the study area in central Shaanxi Province, China (Xu *et al.* 2016)

(a) Loess deposits in Jingyang area

(b) In situ cracks in horizontal fields

Fig. 2 Field investigation of cracks in clayey loess

(Avila 2004, Kodikara *et al.* 2013, Wei *et al.* 2016). In addition, many researchers have tried to model the formation and evolution of cracks in soils, using finite element method (FEM) or discrete element method (DEM). Generally, cohesive fracture theory and interface elements are often considered in FEM method to model the cracking process (Youshida *et al.* 2004, Trabelsi *et al.* 2012, Hirobe *et al.* 2017). However, these methods are often limited by the lack of experimental data.

In the last twenty years, with the development of image processing techniques (for instance, using the software ImageJ), many studies were carried out to measure the evolution of the geometric parameters of cracks during drying, including length, average width, total area of cracks, etc., even in the case of cracks with complicated geometry and irregular shape (Peng *et al.* 2006, Tang *et al.* 2008, 2011, Lakshmikantha *et al.* 2009, Auvray *et al.* 2014, DeCarlo *et al.* 2014, 2019, Zhang *et al.* 2016, Zhang *et al.* 2019). In that case, the results show the evolution of cracks but lack of information about displacements or strain tensors.

More recently, a more powerful image processing technique appeared, using Digital Image Correlation (DIC) to allow precise determination of local displacements and strains on the surface of the sample. The method consists in dividing the digital image into small areas, then comparing the areas from different images by identifying the similarity of gray characteristic values. Based on the movement information recorded in pixels, the displacements and strains can be calculated. Two-dimensional Digital Image Correlation (DIC) can be performed by different programs, like VIC-2D (Eid *et al.* 2015; Wei *et al.* 2016), Correli[Q4] (Mathieu *et al.* 2011), CMV (Wang *et al.* 2018), and other programs in the background of a finite-element post-processing tool or Matlab (Pan *et al.* 2009; Shannon *et al.* 2015; Abd El-Halim 2017). For instance, Eid *et al.* (2015) studied the shrinkage process and drying-induced cracks in a natural silt, Wang *et al.* (2018) analyzed the nucleation and propagation mechanisms of cracks in a natural high plasticity clayey soil, Li *et al.* (2019) measured the tensile strength of a clayey soil.

Many researchers carried out in-situ observations (Willden and Mabey 1961, Kargel *et al.* 1996, Konrad *et al.* 1997, Kodikara *et al.* 2013, Cordero *et al.* 2016) and laboratory experimental studies (Péron 2008, Pasricha *et al.* 2009, Tang *et al.* 2011, Li *et al.* 2016, Wang *et al.* 2016, Wei 2014, Zhang *et al.* 2017, Li *et al.* 2017, Costa *et al.* 2017) of desiccation cracks in different soils. However, investigations about dynamics of crack pattern formation and related mechanisms in complex clayey soils such as loess are less frequent (Lu *et al.* 2015, Zhang *et al.* 2016, Wu *et al.* 2017). The spatio-temporal evolution of the stress field in loess during drying has not been quantitatively characterized, which leads to a gross lack of data on this material. Thus, the relationship between the physical properties of loess and its cracking mechanisms needs to be highlighted.

In a previous paper, Wei *et al.* (2016) analyzed different

mechanisms involved in the formation and propagation of cracks in various laboratory clays ranging from kaolinite to montmorillonite. The objective of the present paper is to (i) show the effect of the mineralogy of a natural clayey loess on its behavior, compared to that of a laboratory clay with similar liquid limit; (ii) highlight the similarity between the crack patterns obtained in the laboratory during the tests that were carried out, and those observed in-situ; (iii) show the importance of the soil-water characteristic curve (SWCC) to correctly interpret and model the results of cracking tests; (iv) define and highlight some little known mechanisms associated to soil cracking, such as crack coalescence, junction and bifurcation.

2. Geological setting of the study site

The site selected for this study is located in Jingyang, Shaanxi Province, northwestern China (Fig. 1). Generally, loess is classified as sandy loess, silty loess and clayey loess (Liu 1965). It is known that loess is transferred by wind so that, nearer to the Mu Us desert, the particle size is coarser, and its density is higher. The particle size becomes finer and finer from the northwest to the southeast. The study site and the sampling location (Fig. 1) are far from the desert, resulting in fine and clayey loess. The tested soil specimens were taken at the surface of the south Jingyang platform that belongs to Middle Pleistocene (Q_2). The samples are classified as Malan Loess in China, which is a typical Aeolian soil. Originally, the samples were at a depth of 50 m below ground level, then the soil was eroded by wind. This soil is characterized by a metastable structure with special geotechnical and physical properties, a relatively low density and high porosity.

The location site belongs to the warm-temperate continental monsoon climate featuring four distinct seasons. The annual average temperature is 13°C with the coldest temperature of -20.8°C in winter (January) and the hottest temperature of 41.4°C in summer (July). The air temperature also varies largely between day and night. The average annual rainfall is about 548.7 mm, with an annual maximum of 829.7 mm. Annual potential evapotranspiration is about 960.6 mm. Because of the changes in air temperature, relative humidity and solar radiation, cracks are very common in loess slopes. Field investigations indicate that lots of cracks exist in foundations and slopes made of loess (Fig. 2(a)). Cracks at the surface of cliffs and in horizontal fields are visually apparent. Hierarchical pattern formation can be observed in-situ in clayey loess, meaning that the cracks are not formed simultaneously, but rather in a sequential and hierarchical way. The pre-existing cells are tessellated successively by new cracks and divided into smaller cells. Rather than uniform spacing or irregular patterns of cracks, the clayey loess is characterized by orthogonal and non-orthogonal patterns of cracks, as shown in Fig. 2(b).

3. Materials and methods

3.1 Soil properties

The clayey loess used in this research was taken from a loess platform in Jingyang, Shaanxi Province, China. Particle size distribution, determined by conventional sieving and sedimentation methods, is shown in Fig. 3. The silt content is equal to 75% and the clay content is 23%. The plastic and liquid limits of the tested soils are 17% and 35%, respectively. The intact dry density is around 1.58-1.59, corresponding a void ratio in the range from 0.72-0.74, and the natural water content is in the range from 18-20% (Xu *et al.* 2017). Table 1 shows the mineralogy of the soil, determined by X-ray diffraction (XRD). The predominant minerals are quartz, albite, calcite and clay, formed of montmorillonite, illite, kaolinite and chlorite (Table 2). On the basis of the Unified Soil Classification System (ASTM 2011), the loess used in this research is classified as clay of low plasticity (CL). Compared to the pure kaolinite studied by Wei *et al.* (2016) that has nearly the same liquid limit, the loess features a very different grain size distribution and mineralogy. In particular, the presence of coarser grains may result in completely different cracking mechanisms as they provide another kind of heterogeneity likely to help in the formation of cracks. Fig. 4(a) shows the typical microstructure of intact specimens obtained by scanning electron microscopy (SEM) images of a rupture surface. It can be seen that many of the particles have a platy shape. Larger voids exist between the skeleton clayey particles or aggregated particles. The microstructures of intact and remolded loess are quite similar (Fig. 4). In addition, the crack patterns observed in the laboratory and in-situ are nearly the same. Therefore, the desiccation tests carried out on remolded loess in this research are significant for in-situ applications.

3.2 Methods of determination of the soil-water characteristics curve (SWCC)

In order to obtain the relation between suction, water content and void ratio on drying path (also called soil-water characteristic curve or shrinkage curve), slurry samples were prepared by mixing dry soils with de-aired water at an initial water content equal to the liquid limit. The slurry specimens were vigorously vibrated for several hours and then equilibrated for at least 24 h to remove air bubbles and enhance homogeneous water distribution. With this preparation technique, the soil was close enough to a "normally consolidated" mechanical state. The soil specimens used to determine the SWCC are quite small, with a volume about 1 cm^3. These small dimensions and the slow rate of drying ensured the absence of cracks in the samples.

In the absence of external mechanical stress, three methods were used to impose suction (s): the tensiometric method, osmotic method, and saturated salt solutions (Wei *et al.* 2016; Li *et al.* 2018). In the small suction values range (i.e., 1 kPa < s < 20 kPa), sintered glass tensiometric plates were used and suction resulted from a height difference between the sample and the free end of the water column, 10 cm to 2 m below. In the intermediate suctions range (i.e., 100 kPa < s < 1500 kPa), the soil specimens were put in tightly sealed dialysis membranes, then they were submerged in polyethylene glycol 20 000 (PEG) until

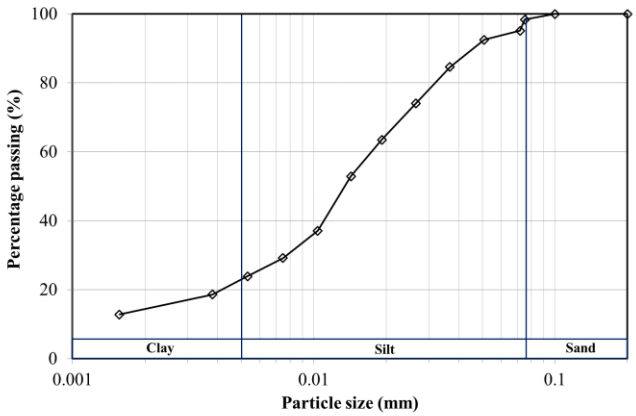

Fig. 3 Particle size distribution of loess samples in Jingyang, China

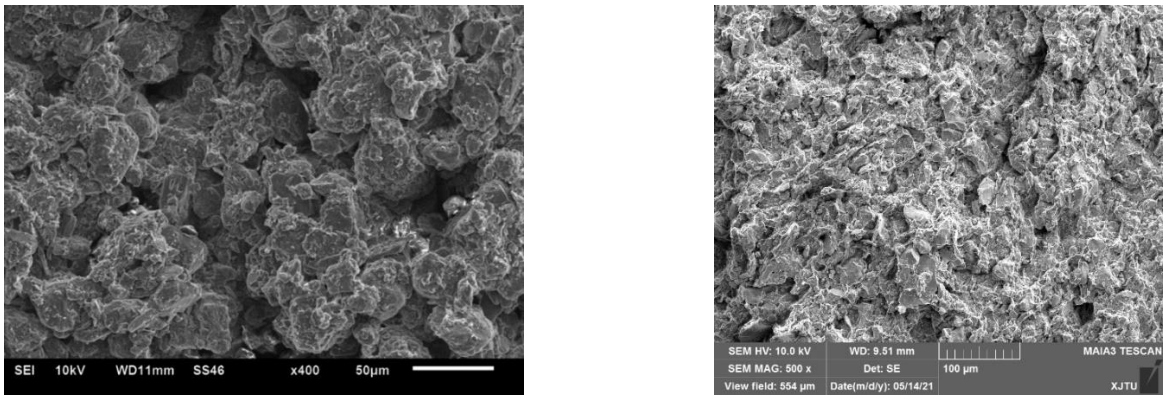

(a) (b)

Fig. 4 SEM photos of the microstructures of the (a) intact clayey loess (Xu *et al.* 2016), and (b) remolded clayey loess, at similar magnitudes

Table 1 Index properties of tested loess specimens

Sample property	Value
Specific gravity	2.69
Liquid limit (%)	36
Plastic limit (%)	17
Gravel content (≥4.75 mm) (%)	0
Sand content (4.75-0.075 mm) (%)	2
Silt content (0.075-0.002 mm) (%)	75
Clay content (≤0.002 mm) (%)	23
Unified Soil Classification System (ASTM 2011)	CL

Table 2 XRD analysis of the clayey loess (Xu *et al.* 2017)

Non-clay minerals (%)	Quartz	Albite	Potassium feldspar	Calcite	Dolomite	Hornblende
	35.1	14.9	0.9	16.5	2.3	1.1
Clay minerals (%)	Montmorillonite		Illite	Kaolinite		Chlorite
	4.4		15.5	3.2		6.1

equilibrium between osmotic pressure and suction was obtained. In the high suction values range (i.e., 5 MPa < s < 500 MPa), the soil specimens were put in a desiccator. At a given temperature, the suction of the specimen slowly evolves toward an equilibrium with the relative humidity in the desiccator.

Once they had reached equilibrium, the specimens were first weighed in air. Then they were put in a non-wetting oil to measure their external volume. Finally, the samples were dried and their void ratio, water content and degree of these

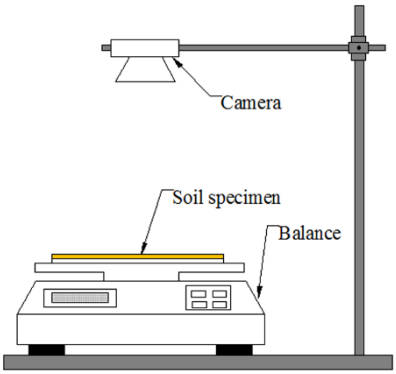

Fig. 5 Schematic drawing of the experimental layout

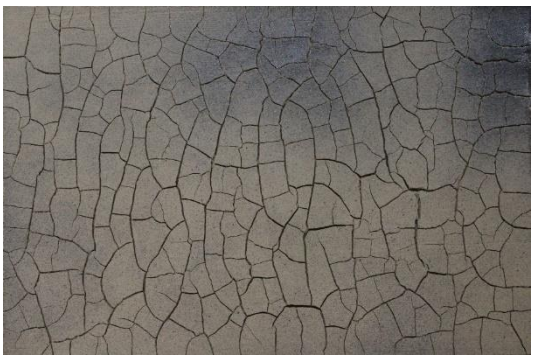

Fig. 6 Typical crack patterns at the end of desiccation (thickness = 4 mm, t = 30 h)

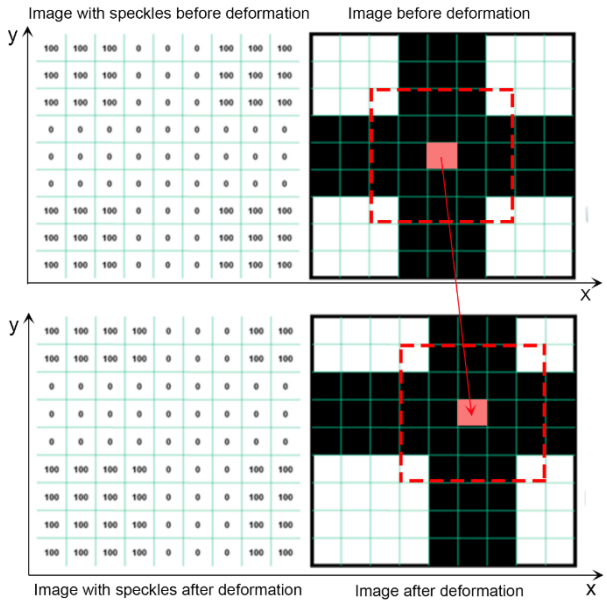

Fig. 7 Implementation of DIC analysis (pixel 100 = white, pixel 0 = black)

saturation were calculated. The results of measurements are presented in section 4.1.

3.3 Free desiccation tests with Digital Image Correlation method

3.3.1 Experimental setup and description of the tests

In-situ, clayey loess is deposited with a loose structure and large pores, in a metastable state. In the presence of water (rain, underground water etc.), loess is subjected to an important erosion characterized by significant deformations due to the partial collapse of the structure, depending on the applied stress. Then, the soil may be assumed to progressively tend towards a "normally consolidated" state. On another hand, free drying tests on intact loess are very difficult to carry out in the laboratory, due to the difficulty of cutting a thin layer of soil of constant thickness.

Therefore, in order to simulate the in-situ desiccation process and to observe the formation and propagation of cracks, clayey loess soil samples were prepared as a slurry, at a water content equal to the liquid limit, i.e. in a normally consolidated state. Free drying tests were performed in an environmental chamber at a temperature of 25°C and RH of 30 ± 5%. The experimental set-up is presented in Fig. 5. A thin layer of clayey loess slurry of constant thickness (4 mm) was spread on a smooth rectangular Plexiglas support (300 mm in length × 200 mm in width) that is non-wettable by water. The adhesion forces between the support and the soil were assumed to be significantly smaller than the suction forces. The crack patterns obtained in laboratory tests, with frequent "T" and "Y" shape (Fig. 6), are quite similar to those observed in-situ (Fig. 2(b)), proving the validity of the approach. In addition, Lu *et al.* (2005) and Zhang *et al.* (2017) also highlighted the similarity of cracking patterns of loess in northwestern China between in-situ observations and laboratory tests on remolded specimens.

This experimental set-up allows observing the cracks initiation and propagation at the surface of the soil sample by taking photos with a digital camera at regular intervals (10 min). The Digital Image Correlation method (DIC) was used to analyze a series of photos of the sample during the drying process. A random dot patterns (speckled pattern) needs to be prepared on the surface of the specimen so that the program can calculate the displacements and strains of the points (Fig. 7). The dotted-speckle patterns were made by black paint that was sprayed from a distance of about 50 cm. DIC enables to correlate subsets of pixels in the reference image with their homologous ones in the deformed image. The computer software VIC-2D was used to calculate the displacements of the pixels between the reference and deformed images. Then, the displacement and strain contour maps were obtained, as explained in detail in Wei *et al.* (2016) and Wei *et al.* (2021). The results were used to analyze precisely the local behavior of the loess during desiccation, the influence of the sample heterogeneities etc. However, in the close neighborhood of the cracks, the continuity conditions are no longer satisfied and the program is not able to calculate the displacements. These zones of error are shown in grey in Fig. 10.

3.3.2 Calculation of strains and displacements and principle of measurement

With the program Vic-2D, there are 5 outputs, two displacements and three strains:

(i) U (mm) – longitudinal displacement (along x axis), with respect to the reference image;

(ii) V (mm) – transversal displacement (along y axis);

(iii) ε_{xx} (%) – normal component of strain in the x

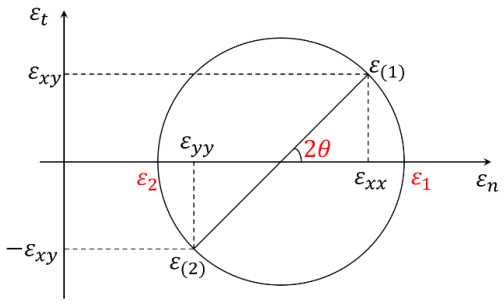

Fig. 8 Interpretation of Mohr circle

direction;

(iv) ε_{yy} (%) – normal component of strain in the y direction;

(v) ε_{xy} (%) – tangential component of strain (distortion).

The results of the measurements are presented as strains contour maps and displacements vectors. Images are taken at a regular interval of 10 minutes during the free desiccation tests. The dimensions of the images are 2000×1382 pixels. With Vic-2D the analysis is carried out with a subset zone of 21×21 pixels. In order to better observe and analyze the deformations derived from VIC-2D, a principal deformation map was obtained with the interpretation of the Mohr circle (Fig. 8). The major and minor principal strains, named ε_1 and ε_2, respectively, and the angle of the major principal strains with respect to the x axis, named θ, can be derived from the results of VIC-2D (ε_{xx}, ε_{yy} and ε_{xy}) using the following equations:

$$\varepsilon_1 = \frac{\varepsilon_{xx} + \varepsilon_{yy}}{2} + \sqrt{(\frac{\varepsilon_{xx} - \varepsilon_{yy}}{2})^2 + {\varepsilon_{xy}}^2} \quad (1)$$

$$\varepsilon_2 = \frac{\varepsilon_{xx} + \varepsilon_{yy}}{2} - \sqrt{\left(\frac{\varepsilon_{xx} - \varepsilon_{yy}}{2}\right)^2 + {\varepsilon_{xy}}^2} \quad (2)$$

$$\theta = \frac{1}{2} arctg \frac{2\varepsilon_{xy}}{\varepsilon_{xx} - \varepsilon_{yy}} \quad (3)$$

Knowing the shrinkage strains ε_{ss} allows to calculate the "mechanical" strains acting on the cracks during drying that represent the factors directly responsible of cracking. They can be derived from the total strains determined by DIC using the following expressions (Bazant and Wittman 1982):

$$\varepsilon_1^m = \varepsilon_1 - \varepsilon_{ss} \quad (4)$$

$$\varepsilon_2^m = \varepsilon_2 - \varepsilon_{ss} \quad (5)$$

$$\theta^m = \theta \quad (6)$$

With the values of ε_1^m, ε_2^m and θ^m, the tensors of local principal "mechanical" deformations are calculated by a program based on MatLab. The principal "mechanical" strain tensors are plotted as small crosses whose arm lengths are proportional to ε_1^m and ε_2^m, respectively, and whose orientation of the major principal strain with respect to the horizontal direction is equal to θ^m. The red color indicates that the principal strains are extensions (positive) while the blue color represents the compressions (negative). The volumetric strain ε_v is calculated by the following relation:

$$\varepsilon_v = \varepsilon_h + \varepsilon_l + \varepsilon_z \quad (7)$$

where ε_h and ε_l represent the principal strains in the transversal and longitudinal directions of the horizontal plane, respectively, and ε_z is the vertical principal strain. The anisotropy ratio η is defined as $\varepsilon_z/\varepsilon_h$. In the research of Bronswijk (1990), η is approximately equal to 0.8. Cornelis *et al.* (2006) carried out desiccation tests on clayey soils and found that η ranges from 1 to infinite. In the desiccation study of Péron *et al.* (2009), the anisotropy ratio η is about 2.5. Auvray *et al.* (2014) performed tests and found that η is close to 2. According to the above researches, the vertical strain is usually larger than the horizontal one but it is still difficult to give a definite value of the anisotropy ratio η. Taking into account the dispersion of the experimental results, an anisotropy ratio η of 2 was selected in this research.

Measurements showed that the shrinkage strains are generally similar in the transversal and longitudinal directions of the horizontal plane (Wei 2014), so that Eq. (7) can be expressed as follows:

$$\varepsilon_v = 2\varepsilon_h + \varepsilon_z = 4\varepsilon_h \text{ and } \varepsilon_h = \frac{\varepsilon_v}{4} \quad (8)$$

In this equation, ε_h represents the uniaxial shrinkage strain ε_{ss} that can be expressed by the following equation:

$$\varepsilon_{ss} = \frac{\Delta e}{4(1 + e_0)} \quad (9)$$

where e_0 is the initial void ratio; Δe is the difference between e_0 and the actual void ratio e, which is derived from the measured water content and the *w*-*e* shrinkage curve.

4. Results

4.1 Soil-water characteristic curves (SWCC) of the clayey loess

Fig. 9 shows the results of a drying test performed on the small samples of clayey loess that were prepared at an initial water content equal to the liquid limit of the soil, then subjected to increasing suctions. These results are presented in 4 planes: (a) void ratio e versus water content w; (b) void ratio e versus suction s; (c) water content w versus suction s and (d) degree of saturation S_r versus suction s. The results highlight several domains in the drying path: (1) a first domain in which the loess remains saturated up to the air entry suction; (2) a second domain where desaturation begins, but remains limited; (3) a third phase where the void ratio is nearly constant, and the degree of saturation decreases rapidly to reach nearly 0. The initial void ratio of the soil was approximately equal to 0.81 and decreased during drying. The curve first follows the saturation line

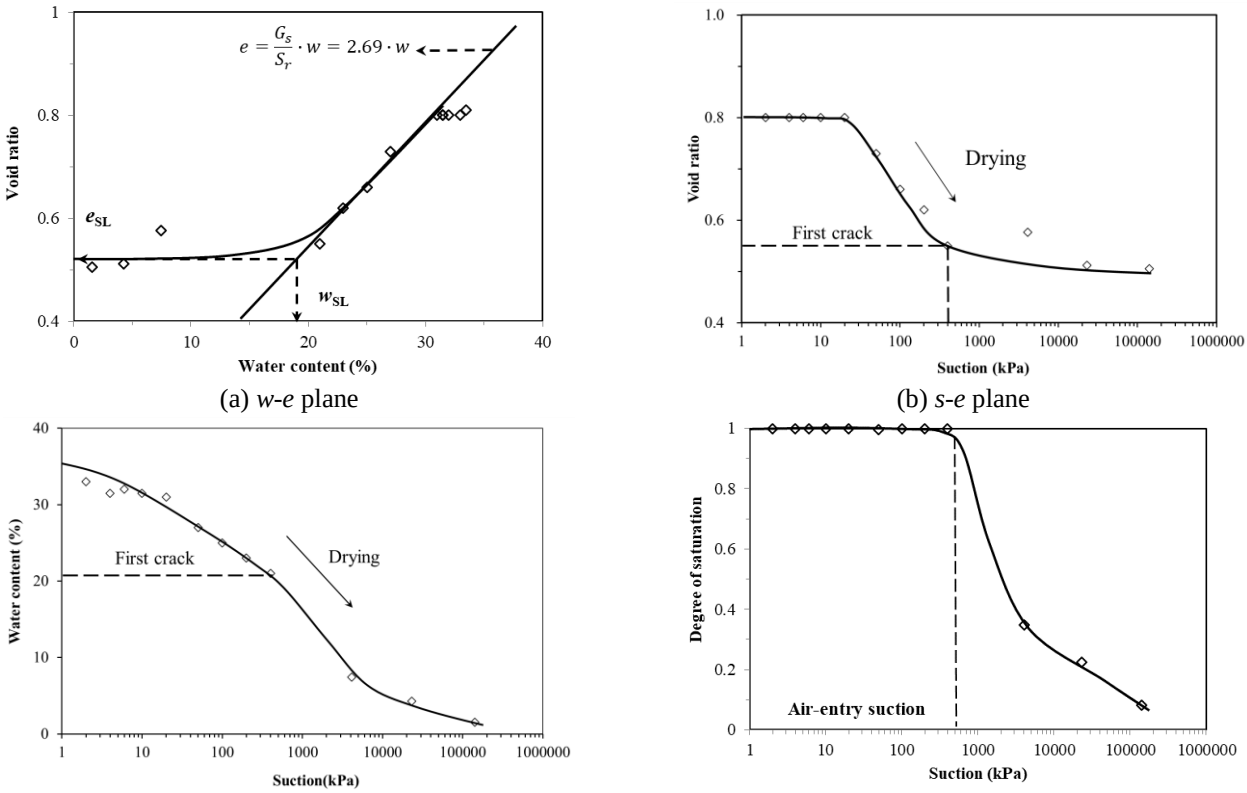

(a) *w*-*e* plane (b) *s*-*e* plane

(c) *s*-*w* plane (d) *s*-S_r plane

Fig. 9 Drying path of Jingyang clayey loess slurry

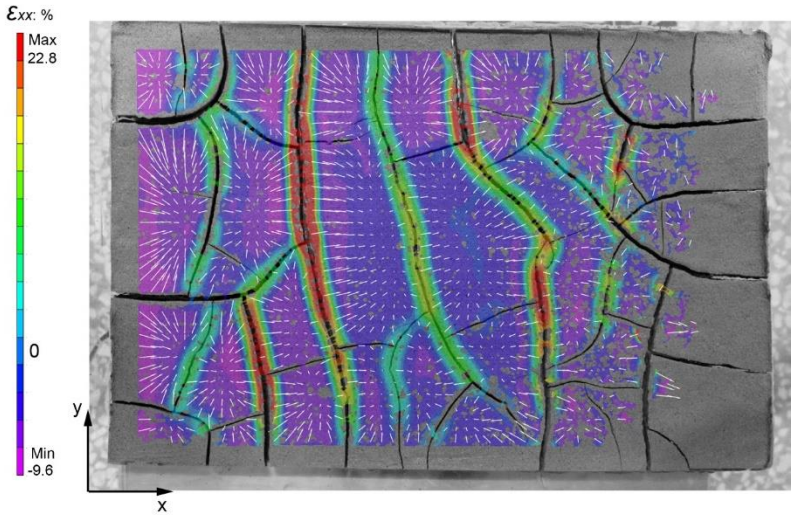

Fig. 10 Contour map of strains ε_{xx} and displacement vectors of loess (thickness = 10 mm; t = 35h)

($e = G_s \cdot w$) in the *w*-*e* plane as long as the soil remains saturated (Fig. 9(a)), then tends toward a horizontal plateau. The shrinkage limit water content (w_{SL}) is about 18%, which is close to the plasticity limit as usual. The clayey loess remains saturated up to 500 kPa. The water content w and degree of saturation S_r gradually decrease under increasing suction s. The suction and degree of saturation for which the formation of the first crack was detected is shown in Fig. 9(c). The first crack initiated when the soil was still fully saturated, at a suction approximately equal to 300 kPa in the case of this specimen.

As expressed by Eq. (9), the shrinkage deformation ε_{ss} can be deduced from the *w*-*e* results (Fig. 9(a)). The variation of water content as a function of time (*t*-*w* result) can be obtained with the desiccation experimental set-up. For example, the first crack appeared at t = 10 h when the water content w was equal to 22%, and the suction equal to 400 kPa. Therefore, the combination of *t*-*w* and *s*-*w* results allows calculating the variation of suction s as a function of time on the drying path. The in-situ desiccation process can be simulated under laboratory conditions on the basis of the SWCC results. Introducing suction as a parameter of drying

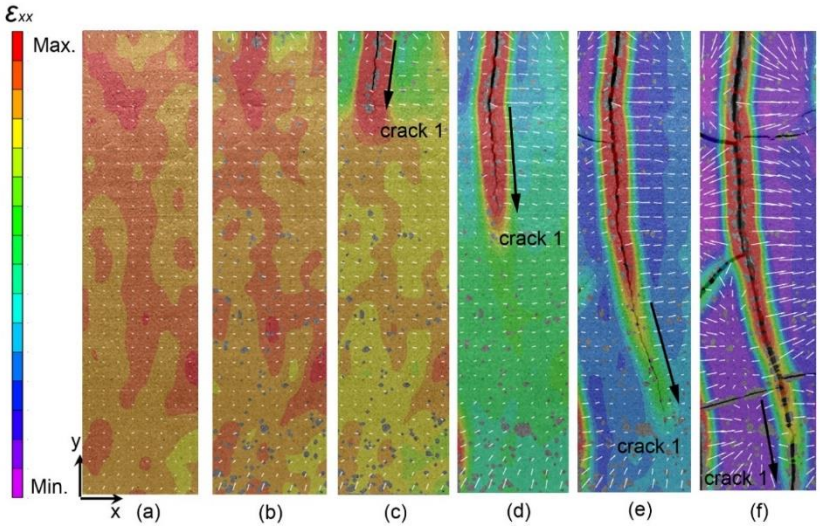

Fig. 11 Illustration of the propagation of cracks at different times: (a) t = 10 h, (b) t = 15 h, (c) t = 18 h, (d) t = 21 h, (e) t = 25 h and (f) t = 35 h

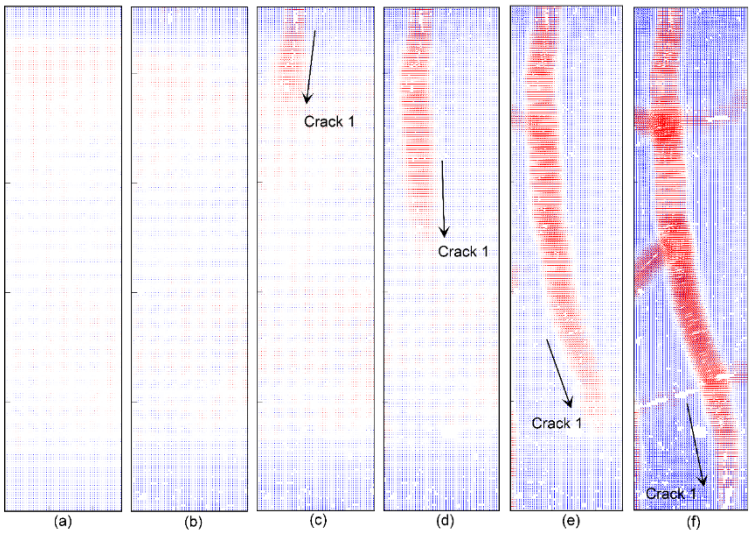

Fig. 12 Schemas of principal "mechanical" strains at different times: (a) t = 10 h, (b) t = 15 h, (c) t = 18 h, (d) t = 21 h, (e) t = 25 h and (f) t = 35 h

is important as the constitutive law of soil is directly related to suction rather than to the state parameters. Models of soil cracking use suction to determine the strength envelope of the soil during the drying process.

4.2 Determination of local strains and displacements fields

Fig. 10 shows the contour map of ε_{xx} and the total displacement vectors (white arrows) at the end of a drying test (after 35 hours). The drying shrinkage ε_{ss} of clayey loess at that time, derived from Eq. (9) for the corresponding value of water content, is equal to -4.3%. The minimum negative ε_{xx} is shown in Fig. 10 (in purple), with a value of -9.6%. It is mainly located at the left boundary of the soil sample and in the inner crack cells. Generally, the direction of the displacements is towards the center of crack cells. The maximum positive ε_{xx} (in red), which is equal to 22.8%, is mostly located at the boundaries of cracks. Most positive strains (in green or yellow) are distributed in the vicinity of cracks, in the range from 0% to 22.8%. The gradual change from positive values to negative values (red, green to purple) indicates that cracks are mainly caused by extensions. Shrinkage often appears in the center of each crack cell, where compressions are detected. On the right side of the soil sample, the grey zones indicate zones in which correlation could not be achieved, possibly because of changes of lighting during the tests. These grey zones cannot be analyzed.

Table 3 Drying shrinkage strains ε_{ss}, maximum and minimum ε_{xx} of clayey loess at different times (corresponding to Figs. 11 and 12)

Time	t = 10 h	t = 15 h	t = 18 h	t = 21 h	t = 25 h	t = 35 h
ε_{ss} (%)	-3.59	-3.80	-3.87	-4.01	-4.14	-4.28
Max. ε_{xx} (%)	0.5	0.9	1.5	6.0	12.8	22.8
Min. ε_{xx} (%)	-3.5	-4.75	-5.5	-6.7	-7.4	-9.6

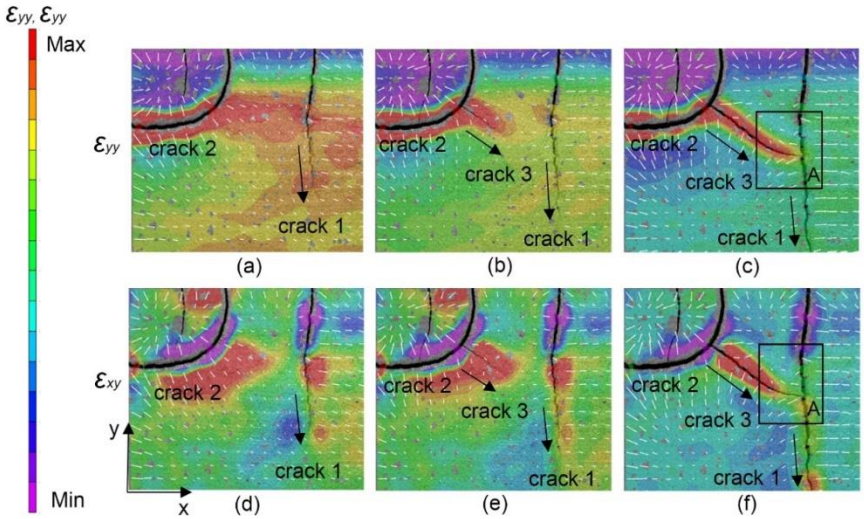

Fig. 13 Phenomenon of junction at different times (max. and min. ε_{yy}, ε_{xy} in Table 4): (a) t = 20 h, (b) t = 21 h, (c) t = 25 h, (d) t = 20 h, (e) t = 21 h and (f) t = 25 h

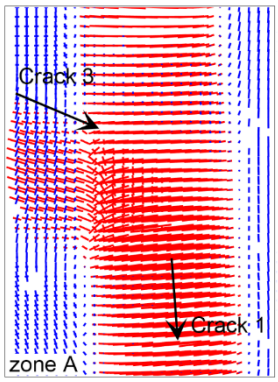

Fig. 14 Representation of principal "mechanical" strains in zone *A* (t = 25 h)

Table 4 Drying shrinkage strains ε_{ss}, maximum and minimum ε_{yy}, ε_{xy} of clayey loess at different times (corresponding to Figs. 13 and 14)

Time	t = 20 h	t = 21 h	t = 25 h
ε_{ss}: %	-4.0	-4.01	-4.14
Max. ε_{yy} (%)	1.1	2.6	7.0
Min. ε_{yy} (%)	-6.5	-6.6	-7.3
Max. ε_{xy} (%)	1.1	1.3	4.2
Min. ε_{xy} (%)	-1.5	-1.7	-2.9

4.3 Mechanics of cracks

4.3.1 Propagation of cracks

Cracks in loess were observed in this study at different times during the free desiccation tests. From the contour map of ε_{xx}, a zone of interest was chosen to analyze the propagation of cracks (Fig. 11). Schemas of principal "mechanical" strains are shown in Fig. 12. Since the direction of crack 1 is nearly transversal, its propagation can be more clearly interpreted with the presentation of the strains ε_{xx}. Maximum and minimum ε_{xx} at different times are summarized in Table 3. Shrinkage strains ε_{ss} were also calculated for the different times and water contents.

At the beginning of drying (t = 10 h), no obvious crack is observed in the zone of interest. At the present resolution ratio, the transversal and longitudinal strains are relatively small, as well as the displacement vectors, which are not visible. Strains ε_{xx} in this zone are between -3.5% and 0.5%. The principal "mechanical" strains are very small (Figs. 11(a)-12(a)). At t = 15 h, the strains ε_{xx} gradually increase and the first crack in this zone begins to appear. There are mainly extensions in the vicinity of crack 1. The maximum and minimum strains ε_{xx} range from 0.9% to -4.8% (Figs. 11(b)-12(b)). After 3 hours (t = 18 h), crack 1 propagates downwards. Maximum and minimum strains ε_{xx} are 1.5% and -5.5%, respectively, larger than those at t = 15 h. Around crack 1, extensions are more obvious, as can be seen from the principal "mechanical" strains map, where the blue vectors indicate compressions and the red vectors represent extensions (Figs. 11(c)-12(c)). At t = 21 h, crack 1 propagates much further. Fig. 12(d) shows that, at the tip of crack 1, the direction of extensions is perpendicular to the direction of crack 1. At t = 25 h, the maximum strain ε_{xx} reaches 12.8% and becomes much larger (in absolute value) than the minimum strain, nearly the double of the value at t = 21 h. Displacements near the main crack 1 remain large as can be evidenced by the white vectors (Figs. 11(e)-12(e)). At t = 35 h, the main crack 1 propagates further and crosses the limits of the chosen zone. The maximum strain ε_{xxmax} increases dramatically near the vicinity of the main crack 4 and the minimum strain ε_{xxmin} increases (in absolute value) just a little. The average width of the main crack 1 increases, which can be indicated by the displacement vectors. It is obvious that the extensions are larger when they are closer to crack 1 (Figs. 11(f)-12(f)). The strains ε_{xx} vary gradually from extensions to compressions, from the vicinity of the main crack to the inner area of the crack cells.

4.3.2 Evolution of cracks

During desiccation, phenomena of junction, coalescence

and bifurcations of cracks were observed in clayey loess.

Junction of cracks

The *junction* of two cracks happens when one crack initiates, propagates toward another one and joins it more or less perpendicularly. This process finally leads to the failure of the soil block. After the junction of two cracks, the strain energy near the junction point is expected to be very small. However, to our knowledge, the mechanism of cracking junction in soil has been little discussed, although this phenomenon has received attention in other materials like rocks or metals (Daux *et al.* 2000, Liang *et al.* 2003, Kobayashi *et al.* 2008, Sun *et al.* 2018, Sun *et al.* 2019).

Junction between crack 1 and crack 2 is shown in Fig. 13. The direction of crack 3 that connects these two cracks is toward the east-southeast. Drying shrinkage strains, and maximum and minimum ε_{yy} at different times are summarized in Table 4. Maximum and minimum shear strains ε_{xy} are also indicated to identify the cracking mode of crack 3. As described in Fig. 11, crack 1 propagates downwards. At t = 20 h, crack 2 has formed with a curved shape. Between cracks 1 and 2, there is no obvious crack. Meanwhile, strains ε_{yy} between these two cracks are relatively larger than in the other areas. It is noticed that, around the middle of crack 3, the shear strains ε_{xy} reach 1.1%, which is larger than in the other areas (Figs. 13(a)-13(d)). One hour later, at t = 21 h, crack 3 initiates from the middle of the preexisting crack 2. In the vicinity of crack 3, ε_{yy} and ε_{xy} increase and remain larger than in the other areas (Figs. 13(b)-13(e)). At t = 25 h, crack 3 propagates towards the southeast and is already connected with the main crack 1 (Figs. 13(c)-13(f)), so that a network of cracks has been formed. The principal "mechanical" strains map in zone *A* is shown in Fig. 14. In the vicinity of crack 3, the extensional principal "mechanical" strains are relatively large, with a direction parallel to the direction of crack 3. At the junction point of cracks 1 and 3, the direction of extensional principal "mechanical" strains turns to be perpendicular to the direction of crack 1, which signifies that, at the tip of these cracks, there are mainly extensions (Fig. 14). This can also be verified by the directions of the displacement vectors shown in Fig. 11(e). Thus, the mode of crack 3 is classified as "mixed opening-sliding mode". The phenomenon of junction is the most common in clayey loess during free desiccation, and it is characterized by the formation of more or less orthogonal patterns of cracks.

Coalescence of cracks

In soil mechanics, there is not a clear definition of *coalescence*. In this research, coalescence is defined as the development of two cracks propagating toward one another and joining in the vicinity of their tips. Experimental and numerical works on the coalescence of cracks in concrete and rocks have been carried out by many researchers (Wong *et al.* 2001, Sagong *et al.* 2002, Park *et al.* 2009, Lee *et al.* 2011, Tang *et al.* 2011, Zhou *et al.* 2015, 2016, Sun *et al.* 2019). In brittle materials, coalescence of cracks may be either in tensile mode or shear mode, or a combination of both modes (Reyes *et al.* 1991, Tang *et al.* 1998, Bobet *et al.* 1998, Sagong *et al.* 2002, Shen *et al.* 2018), resulting in different crack patterns. In free desiccation tests on clayey soils, during drying, existing cracks propagate further towards each other, which leads to coalescence. The relationship between the crack patterns and the type of coalescence requires to be interpreted. Coalescence of cracks is the dominant controlling source that leads to macroscopic failure in geomaterials (Bombolaksi 1963, Li *et al.* 2005, Park *et al.* 2010, Bagheripour *et al.* 2011, Panaghi *et al.* 2015). In loess, two different types of coalescence were observed (Table 5).

Table 5 Crack coalescence patterns in clayey loess during free desiccation (The solid lines represent the existing cracks and the dotted lines are for the propagation of the cracks)

Type	Schematic of coalescence	Description of coalescence	Mode of coalescence
I	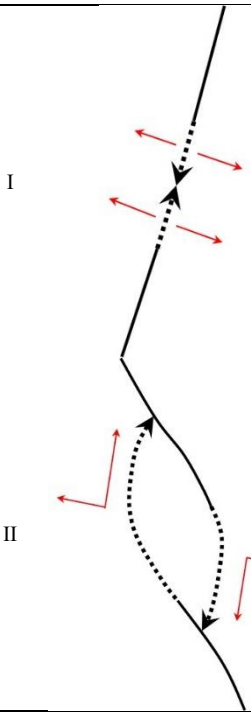	Type I of coalescing crack: tension crack in opening mode. Initiation position: existing crack tips.	tension
II		Type II of coalescing crack: crack in mixed opening-shearing mode. Initiation position: existing crack tips.	Shearing + tension

Coalescence type I:

An example of coalescence type I is presented in Figs. 15 and 16. The shrinkage strains ε_{ss} calculated at the different times are shown in Table 6. At t = 26 h, in the zone of interest, the maximum and minimum ε_{xx} are 14.3% and -7.6% respectively. Cracks 4 and 5, which will coalesce later, are not yet visible. Otherwise, at the initiation points of these two cracks, ε_{xx} are relatively larger than in the neighboring areas (Fig. 15(a)). At t =27 h, cracks 4 and 5 appear, with directions that are nearly southeastern and northwestern, respectively (Fig. 15(b)). One hour later, at t = 28 h, with gradually increasing ε_{xx}, it seems that cracks 4 and 5 propagate rapidly and move towards each other. The distance between them is smaller (Fig. 15(c)). It can be seen from the principal "mechanical" strains map that the extensions are perpendicular to the propagation direction of crack 4 (Figs. 16(a)-(b)). At t = 30 h, the ε_{xx} still increase a little and cracks 4 and 5 connect together (Fig. 15(d)). Cracks 4 and 5 propagate in opening mode as shown in Figs. 16(c)-(d), which confirms that the coalescence is generated by tensile cracks. During the coalescence process, more cracks appear and form a crack network.

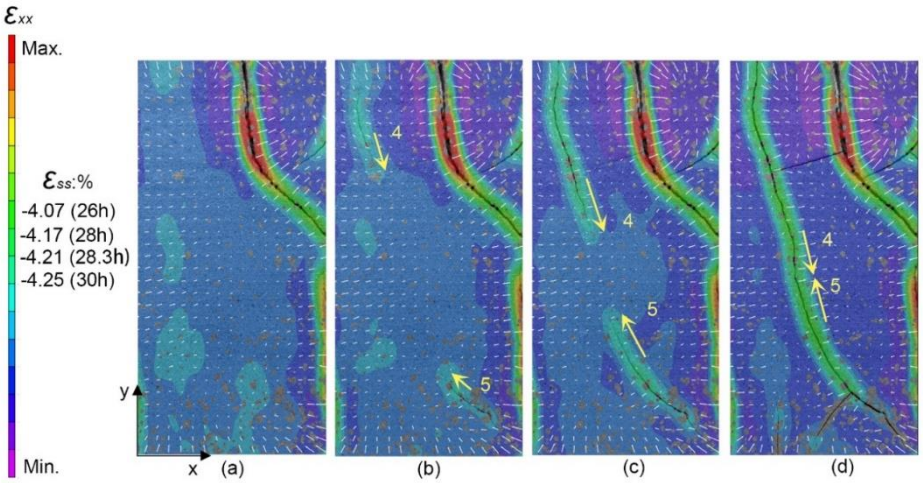

Fig. 15 Coalescence type I at different times (max. and min. ε_{xx} in Table 6): (a) t = 26 h, (b) t = 27 h, (c) t = 28 h and (d) t = 30 h

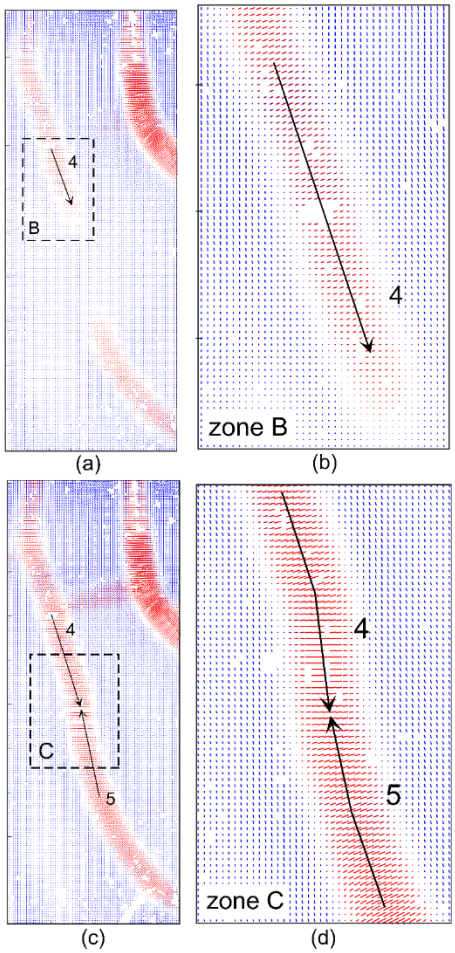

Fig. 16 Schemas of principal "mechanical" strains at different times and different scales: (a) t = 28 h, (b) zoom of zone *B* at t = 28 h, (c) t = 30 h and (d) zoom of zone *C* at t = 30 h

Coalescence type II:

As shown in Figs. 17(f)-17(l), the coalescence type II occurs in the case of two moderately misaligned cracks, like cracks 6 and 7. These cracks propagate so that their closest tips move independently of each other for a small distance before turning and evolving towards the opposite crack. This leaves a small island between these two cracks. At t = 21.5 h, cracks 6 and 7 propagate in opposite directions. With time, crack 6 changes its direction towards southeast and these two cracks propagate further. In the neighborhood of the cracks, ε_{xx} and ε_{xy} are relatively larger than in the other areas (Figs. 17(b), 17(c), 17(h), 17(i)). By contrast

Table 6 Drying shrinkage strains ε_{ss}, maximum and minimum ε_{xx} of clayey loess at different times (corresponding to Figs. 15 and 16)

Time	t = 26 h	t = 27 h	t = 28 h	t = 30 h
ε_{ss} (%)	-4.07	-4.1	-4.17	-4.25
Max. ε_{xx} (%)	14.3	16.3	16.8	18.2
Min. ε_{xx} (%)	-7.6	-8.1	-8.2	-8.6

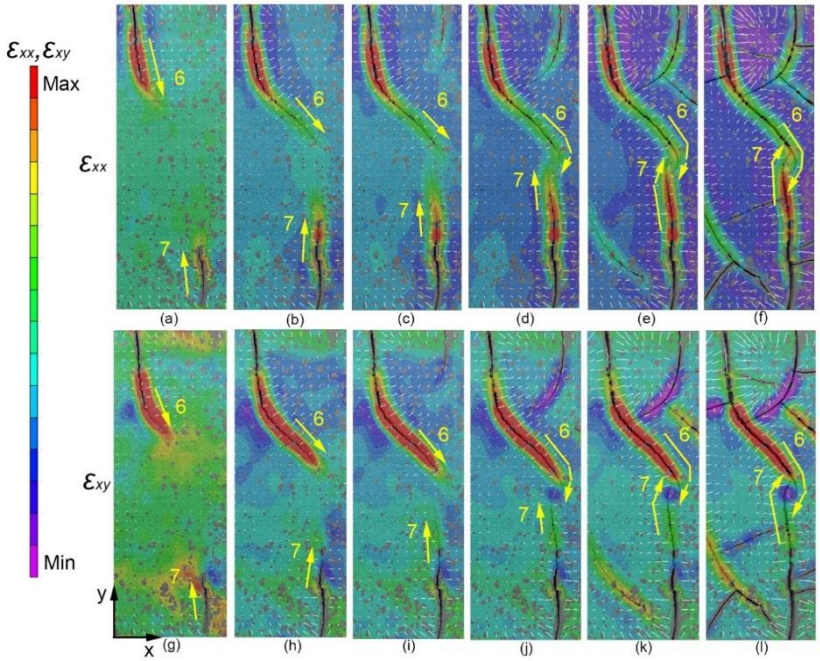

Fig. 17 Coalescence type II at different times (max. and min. ε_{xx}, ε_{xy} in Table 7): (a) t = 21.5 h, (b) t = 23.5 h, (c) t = 24.17 h; (d) t = 25.3 h, (e) t = 28 h, (f) t = 32.5 h, (g) t = 21.5 h, (h) t = 23.5 h, (i) t = 24.17 h, (j) t = 25.3 h, (k) t = 28 h and (l) t = 32.5 h

Table 7 Drying shrinkage strains ε_{ss}, maximum and minimum ε_{xx}, ε_{xy} of clayey loess at different times (corresponding to Figs. 17 and 18)

Time	t = 21.5 h	t = 23.5 h	t = 24.17 h	t = 25.3 h	t = 28 h	t = 32.5 h
ε_{ss} (%)	-4.02	-4.09	-4.12	-4.14	-4.17	-4.26
Max. ε_{xx} (%)	6.7	10.6	11.6	13.4	16.3	21.2
Min. ε_{xx} (%)	-6.9	-7.1	-7.3	-7.4	-8.1	-9.4
Max. ε_{xy} (%)	1.5	3.1	3.6	4.3	5.8	8.2
Min. ε_{xy} (%)	-1.8	-2.1	-2.4	-3.0	-4.4	-6.0

Table 8 Drying shrinkage strains ε_{ss}, maximum and minimum ε_{xx}, ε_{xy} of clayey loess at different times (corresponding to Figs. 19 and 20)

Time	t = 19.7 h	t = 20.7 h	t = 21.3 h	t = 22.2 h	t = 23 h
ε_{ss} (%)	-3.87	-3.93	-4.01	-4.06	-4.07
Max. ε_{xx} (%)	3.4	5.3	6.6	8.2	9.7
Min. ε_{xx} (%)	-6.3	-6.75	-6.8	-6.9	-7
Max. ε_{xy} (%)	1.11	1.24	1.44	1.88	2.54
Min. ε_{xy} (%)	-1.34	-1.56	-1.8	-1.88	-1.92

with the coalescence type I, at t = 25.3 h, cracks 6 and 7 do not interact with each other directly. Crack 8 propagates directly while crack 6 bypasses the tip of crack 7 before turning (Fig. 17 (d)). This can be illustrated by the principal "mechanical" strains map in Figs. 18(a)-(b) showing that the extensions are parallel to the direction of crack 6. It can also be seen in Fig. 17(j) that, between the tips of cracks 6 and 7, ε_{xy} gradually increases. Otherwise, the direction of crack 6 is perpendicular to the direction of extensions at the tip. For the tip of crack 7, it is the same condition. This means that the coalescence between cracks 6 and 7 is caused by mixed "shearing + tension". At t = 32.5 h, ε_{xx} and ε_{xy} increase in the chosen zone. Crack 7 also changes its direction and connects with crack 7 following a bypassing path. There is a small soil block between them (Figs. 17(f), 17(l), and 18(c), 18(d)). Around the block, the ε_{xy} are quite large. The shrinkage strains ε_{ss} calculated at the different times are shown in Table 7.

Bifurcation of cracks

In physics, a *bifurcation* is the spontaneous modification of the dynamics of a system, under the influence of a very slight modification of at least one of its parameters. During drying, primary cracks tend to initiate from soil surface and propagate downwards and sideways simultaneously, in a

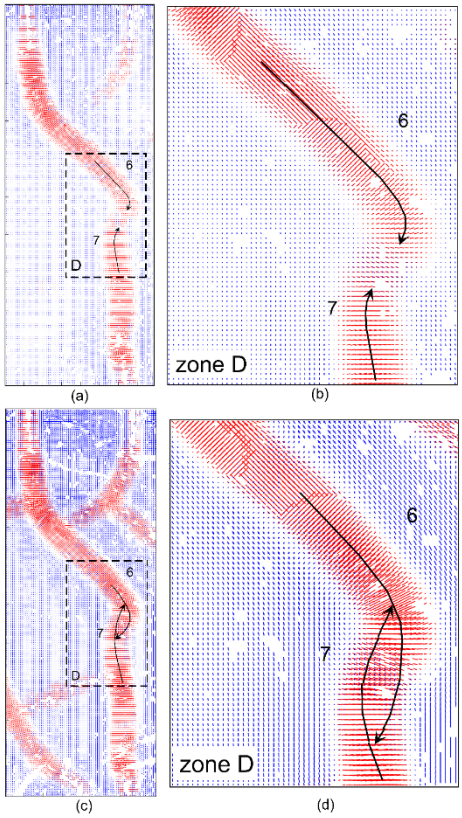

Fig. 18 Schemas of principal "mechanical" strains at different times and different scales: (a) t = 25.3 h, (b) zoom of zone *D* at t = 25.3 h, (c) t = 32.5 h and (d) zoom of zone *D* at t = 32.5 h

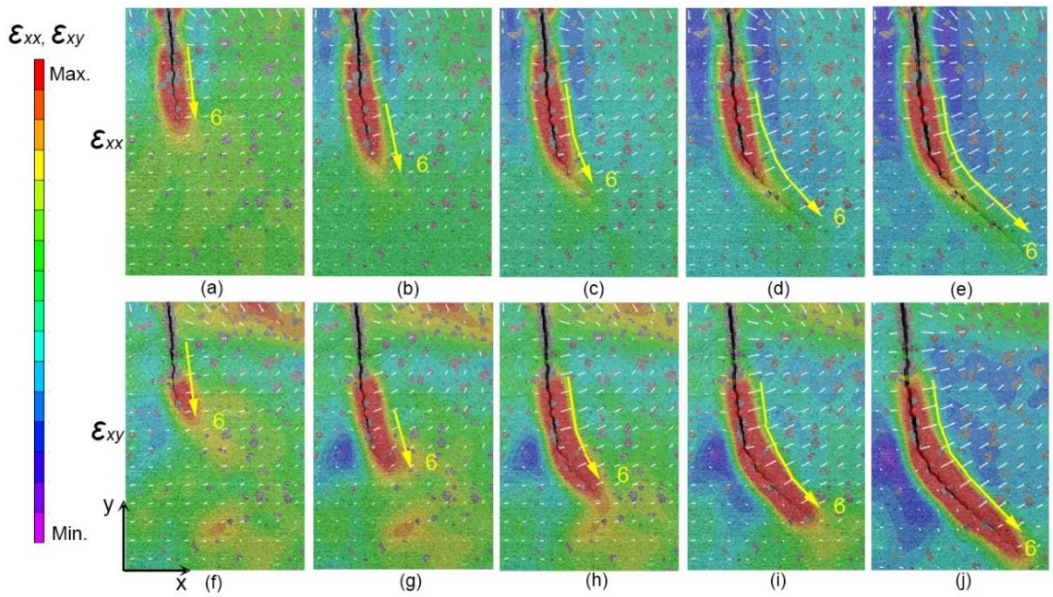

Fig. 19 Bifurcation related to the presence of shear strain on the side of a crack at different times: (a) t = 19.7 h, (b) t = 20.7 h, (c) t = 21.3 h, (d) t = 22.2 h, (e) t = 23 h, (f) t = 19.7 h, (g) t = 20.7 h, (h) t = 21.3 h, (i) t = 22.2 h and (j) t = 23 h

three-dimensional process. The orientation of cracks is random. The propagation path of cracks is perpendicular to tensile strains when a crack is influenced only by tensile strength. However, the direction of the crack will change if there is the action of distortions in the vicinity of the crack. The crack with a changed direction still propagates perpendicularly to the local tensile stress. This phenomenon can be considered to be a bifurcation. Another possible interpretation of bifurcation is that the direction of crack varies to connect with the adjoining tensile area. The initiation points of the bifurcated cracks are far away from each other. Therefore, the crack path is induced by the local stress field rather than the global stress field.

The phenomenon of bifurcation has also been observed

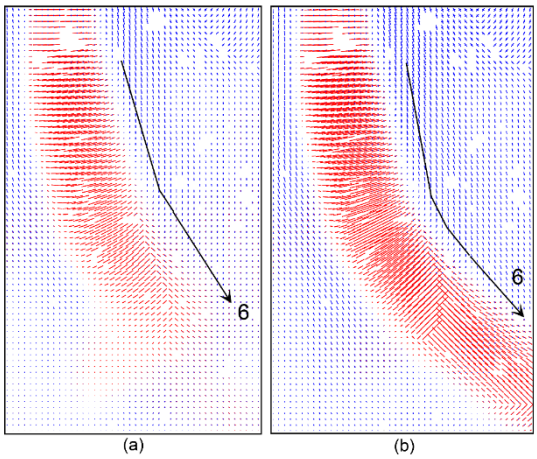

Fig. 20 Schemas of total principal "mechanical" strains at different times: (a) t = 21.3 h and (b) t = 23 h

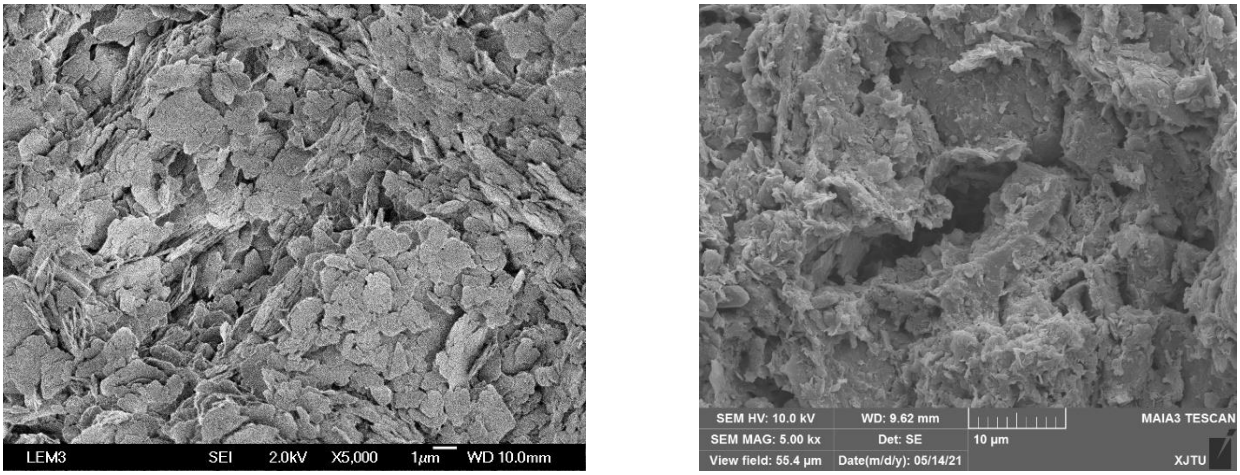

(a) (b)

Fig. 21.SEM photos of the microstructure of (a) kaolin P300 (Wei *et al.* 2013) and (b) the remolded natural loess, at similar magnitudes

in previous sections, for example in the case of crack 6 in Fig. 17. The bifurcation of crack 6 in clayey loess was analyzed at different times (Fig. 19). Schemas of principal "mechanical" strains are shown in Fig. 20. The values of shrinkage strains, maximum and minimum ε_{xx} and ε_{xy} at different times are indicated in Table 8. In the zone of interest, the ε_{xx} are much larger than the ε_{xy} in most parts of the zone at t = 19.7 h. The direction of crack 6 is mainly to the south, and a little east (Fig. 19(a)). After one hour, the maximum ε_{xx} increases, and the maximum and minimum ε_{xy} increase a little. The tip of crack 6 grows further with a little change in direction that is not obvious (Figs. 19(b)-19(g)). Later, crack 6 propagates much further with an obviously changed path. The direction of crack 6 turns towards the southeast to form an angle of about 45° with the previous crack. At the bifurcation point of crack 6, ε_{xy} is very large (in absolute value), about -1.8% (Figs. 19(c)-(h)). It can be seen from Fig. 20(a) that, in the vicinity of the bifurcation point, there are extensions, the direction of which is parallel to the propagation direction of crack 8. Nearly one hour later, at t = 22.2 h, the maximum ε_{xx} increases and reaches 8.2% while crack 8 propagates further. Meanwhile, the maximum ε_{xy} increases a little too. At that time, at the bifurcation point of crack 8, ε_{xy} still remains large, about -1.88% (Fig. 19(i)). At t = 23 h, the maximum and minimum ε_{xy} continuously increase and reach 2.54% and -1.92%, respectively. In the vicinity of crack 6, the ε_{xy} remain large, which can be verified by the schema of the principal "mechanical" strains in Fig. 20(b). It is quite obvious that the direction of crack 6 changes and turns towards southeast (Fig. 19(e)).

4.3.3 Effect of mineralogy on the mechanics of crack

By comparing the results of the present research on clayey loess with those of the study of Wei *et al.* (2016) on various clays, it can be concluded that the final patterns of cracks highly depend on the mineralogy of the soil. Here, the comparison will focus on the clayey loess and the kaolinite that have similar liquid limits (36% for the loess vs. 40% for the kaolinite). However, as mentioned before, the grain size distributions of the two soils are different, with larger grains in the loess.

Microstructure of kaolin P300 and the natural remolded loess are obtained by scanning electron microscopy (SEM)

images (Fig. 21). The aggregate structures can be observed in the natural loess. Among the aggregated particles and clayey particles, large voids exist (Fig. 21(b)). Compared with the natural loess, the kaolinite particles are distinguished by flatter and more compact shape (Fig. 21(a)).

In the research of Wei *et al.* (2016), the surface of kaolin P300 was divided by rough and discontinuous cracks. Separate clods caused by cracks were rarely observed. Crack patterns with "Y" shape were more frequent. The dead-end cracks were common. On the contrary, in this research, the cracks in loess are relatively straight, smooth, and continuous. The shapes of the clods are more regular and most of the clods are quadrangles; the crack segments are generally perpendicular to each other and form "T" and "+" shaped intersections. The crack networks feature very good crack connections and only a few dead-end cracks can be observed. Many soil parameters play a part in the formation of cracks: mineralogy, grain size distribution, rheology, etc. resulting in different crack patterns in different soils.

In both cases, the elementary mechanisms of cracking are quite similar and conform to fracture mechanics theory.

5. Conclusions

In this research, free desiccation tests were performed on a clayey loess taken in Jingyang, Shaanxi Province, China, and analyzed using the Digital Image Correlation method to measure the local strains and displacements. The principal conclusions drawn from this study are as follows:

• In free desiccation tests, if drying is homogenous and there is no other mechanism involved in the process, the displacements are supposed to be toward the center of the specimen and result in no cracks. In reality, because of external restraints or internal flaws, cracks appear in the soil. As pointed out by Amarasiri and Kodikara (2013) and Wei *et al.* (2016), it is the "mechanical" strains, i.e. the difference between of the total strains and the shrinkage strains that should be considered to interpret the initiation and propagation of cracks. In this study, the shrinkage strain ε_{ss} deduced from SWCC results, was used as a reference for extensions and compressions strains.

• The comparison of the results obtained on the clayey loess with those of Wei *et al.* (2016) on a kaolinite highlight that the final patterns of cracks highly depend on the mineralogy of the soils. Crack patterns are different and loess feature relatively straight, smooth, well-connected and continuous cracks compared to kaolinite, in which the cracks were often rough and discontinuous.

• With loess samples of low density, the in-situ desiccation process is well simulated by free desiccation tests carried out in the laboratory on slurry specimens, as evidenced by the very similar crack patterns featuring "T" or "Y" shapes. Different cracking phenomena were observed in the experiments, like, for example, coalescence of cracks that were rarely interpreted in soils: During drying, two cracks propagate toward one another and join by their tips or close to their tips. This phenomenon is defined as coalescence of cracks. In this research, two coalescence types were observed. In addition, initiation, propagation, junction, and bifurcation of cracks were also detected. The initiation of cracks can be predicted by field strain analysis because high extensions are observed before the appearance of cracks. The propagation direction of a crack is perpendicular to extensions when it is led by tension. Bifurcation of crack occurs when there is the action of shear strains in the vicinity of the crack. The crack with a changed direction still propagates perpendicularly to the local tensile strain. The junction of two cracks occurs when one crack initiates and propagates toward another one and joins it more or less perpendicularly.

• In this research, the mechanisms of propagation and coalescence of cracks related to desiccation were highlighted in the case of a clayey loess. In a previous study (Wei 2014, Wei *et al.* 2016), similar phenomena were studied in pure kaolinite clay and mixtures of kaolinite and montmorillonite. All the tests were carried out at an initial water content equal to the limit liquid of the soil, which is nearly the same for kaolinite and loess. Considering the material source of the clayed loess from Mu Us desert, the content of silt and sand in the clayey loess is larger than that of kaolinite and montmorillonite. The crack networks observed in these two researches are quite different highlighting the influence of mineralogy on these phenomena. However, the mechanisms appear to be identical in both materials.

Acknowledgments

This work was supported by Program XU GUANGQI 2018, n°41221YC of Campus France, the National Key Research and Development Program of China (No. 2018YFC1504700), the China Postdoctoral Science Foundation (No. 2017M623180) and the National Natural Science Foundation of Youth (No. 42007278).

References

Abd El-Halim, A.A. (2017), "Image processing technique to assess the use of sugarcane pith to mitigate clayey soil cracks: Laboratory experiment", *Soil Till. Res.*, **169**, 138-145. https://doi.org/10.1016/j.still.2017.02.007.

Amarasiri, A.L. and Kodikara, J.K. (2013), "Numerical modelling of a field desiccation test", *Géotechnique*, **63**(11), 983-986. https://doi.org/10.1680/geot.12.P.010.

ASTM. (2011), Standard practice for classification of soils for engineering purposes (Unified Soil Classification System). ASTM standard D2487. American Society for Testing and Materials, West Conshohocken, Pennsylvania, U.S.A.

Auvray, R., Rosin-Paumier, S., Abdallah, A. and Masrouri, F. (2014), "Quantification of soft soil cracking during suction cycles by image processing", *Eur. J. Environ. Civ. Eng.*, **18**(1), 11–32. https://doi.org/10.1080/19648189.2013.840250.

Avila, G. (2004), "Study of shrinkage and cracking of clays - application to clay in Bogota", Ph.D. Dissertation, Polytechnic University of Catalunya, Barcelona, Spain.

Bagheripour, M., Rahgozar, R. and Pashnesaz, H. (2011), "A complement to Hoek-Brown failure criterion for strength prediction in anisotropic rock", *Geomech. Eng.*, **3**(1), 61-81.

https://doi.org/10.12989/gae.2011.3.1.061.
Baker, R. (1981), "Tensile strength, tension cracks, and stability of slopes", *Soils Found*., **21**(2), 1-17. https://doi.org/10.3208/sandf1972.21.2_1.
Bazant, Z.P. and Wittmann, F.H. (1982), *Creep and Shrinkage in Concrete Structures*, Wiley, New York, U.S.A.
Bobet, A. and Einstein, H.H. (1998), "Fracture coalescence in rock-type materials under uniaxial and biaxial compression", *Int. J. Rock Mech. Min. Sci*., **35**(7), 863-888. https://doi.org/10.1016/s0148-9062(98)00005-9.
Bombolakis, E.G. (1963), "Photoelastic stress analysis of crack propagation within a compressive stress field", Ph.D. Dissertation, Massachusetts Institute of Technology, Cambridge, Massachusetts, U.S.A.
Bronswijk, J.J.B. (1990), "Shrinkage geometry of a heavy clay soil at various stresses", *Soil Sci. Soc. Am. J*., **54**(5), 1500-1502. https://doi.org/10.2136/sssaj1990.03615995005400050048x.
Cornelis, W. M., Corluy, J., Medina, H., Diaz, J., Hartmann, R., Meirvenne, M. V. and Ruiz, M. E. (2006), "Measuring and modeling the soil shrinkage characteristic curve", *Geoderma*, **137**(1-2), 179-191. https://doi.org/10.1016/j.geoderma.2006.08.022.
Cordero, J., Cuadrado, A., Prat, P. and Ledesma, A. (2016), "Description of a field test involving cracking in a drying soil", *Proceedings of the 3rd European Conference on Unsaturated Soils*, Paris, France, December.
Costa, S., Kodikara, J., Barbour, S.L. and Fredlund, D.G. (2017), "Theoretical analysis of desiccation crack spacing of a thin, long soil layer", *Acta Geotechnica*, **13**(1), 39-49. https://doi.org/10.1007/s11440-017-0602-9.
Daux, C., Moes, N., Dolbow, J., Sukumar, N. and Belytschko, T. (2000), "Arbitrary branched and intersecting cracks with the extended finite element method", *Int. J. Numer. Met. Eng*., **48**, 1741-1760. https://doi.org/10.1002/1097-0207(20000830)48:12<1741::aid-nme956>3.0.co;2-l.
DeCarlo, K.F. and Caylor, K.K. (2019), "Biophysical effects on soil crack morphology in a faunally active dryland vertisol", *Geoderma*, **334**,134-145. https://doi.org/10.1016/j.geoderma.2018.07.042.
DeCarlo, K.F. and Shokri, N. (2014), "Salinity effects on cracking morphology and dynamics in 3-D desiccating clays", *Water Resour. Res*., **50**, 3052–3072. https://doi.org/10.1002/2013WR014424.
Eid, J., Taibi, S., Fleureau, J.M. and Hattab, M. (2015), "Drying, cracks and shrinkage evolution of a natural silt intended for a new earth building material. Impact of reinforcement", *Constr. Build. Mater*., **86**(13), 120-132. https://doi.org/10.1016/j.conbuildmat.2015.03.115.
Hirobe, S. and Oguni, K. (2017), "Modeling and numerical investigations for hierarchical pattern formation in desiccation cracking", *Physica D*, **359**, 29-38. https://doi.org/10.1016/j.physd.2017.08.002.
Kargel, J.S., Schreiber Jr, J.F. and Sonett, C.P. (1996), "Mud cracks and dedolomitization in the Wittenoom Dolomite, Hamersley Group, Western Australia", *Global Planet. Change*, **14**, 73-96. https://doi.org/10.1016/0921-8181(95)00055-0.
Kobayashi, S., Inomata, T., Kobayashi, H., Tsurekawa, S. and Watanabe, T. (2008), "Effects of grain boundary- and triple junction-character on intergranular fatigue crack nucleation in polycrystalline aluminum", *J. Mater. Sci*., **43**, 3792-3799. https://doi.org/10.1007/s10853-007-2236-z.
Kodikara, J. and Costa, S. (2013), *Desiccation cracking in clayey Soils: Mechanisms and Modelling* in *Multiphysical Testing of Soils and Shales*, Springer Press, Berlin, Germany, 21-32.
Konrad, J.M. and Ayad, R. (1997), "An idealized framework for the analysis of cohesive soils undergoing desiccation", *Can. Geotech. J*., **34**, 477-488. https://doi.org/10.1139/t97-015.
Lakshmikantha, M.R., Prat, P.C. and Ledesma, A. (2009), "Image analysis for the quantification of a developing crack network on a drying soil", *Geotech. Test. J*., **32**(6), 505-515. https://doi.org/10.1520/GTJ102216.
Lee, F.H., Lo, K.W. and Lee, S.L. (1988), "Tension crack development in soils", *J. Geotech. Eng*., **114**(8), 915-929. https://doi.org/10.1061/(ASCE)0733-9410(1988)114:8(915).
Lee, H.W. and Jeon, S.W. (2011), "An experimental and numerical study of fracture coalescence in pre-cracked specimens under uniaxial compression", *Int. J. Solids Struct*., **48**, 979-999. https://doi.org/10.1016/j.ijsolstr.2010.12.001.
Li, Y.P., Wang, Y.H. and Chen, L.Z. (2005), "Experimental research on pre-cracked marble under compression", *Int. J. Solids Struct*., **42**(9), 2505-2516. https://doi.org/10.1016/j.ijsolstr.2004.09.033.
Li, J.H. and Zhang, L.M. (2011), "Study of desiccation crack initiation and development at ground surface", *Eng. Geol*., **123** (4), 347–358. https://doi.org/10.1016/j.enggeo.2011.09.015.
Li, J.H., Li, L., Chen, R. and Li, D.Q. (2016), "Cracking and vertical preferential flow through landfill clay liners", *Eng. Geol*., **206**, 33-41. https://doi.org/10.1016/j.enggeo.2016.03.006.
Li, J.H., Lu, Z., Guo, L.B. and Zhang, L.M. (2017), "Experimental study on soil-water curve for silty clay with desiccation cracks", *Eng. Geol*., **218**, 70-76. https://doi.org/10.1016/j.enggeo.2017.01.004.
Li, H.D., Tang, C.S., Cheng, Q., Li, S.J., Gong, X.P. and Shi, B. (2019), "Tensile strength of clayey soil and the strain analysis based on image processing techniques", *Eng. Geol*., **253**, 137-148. https://doi.org/10.1016/j.enggeo.2019.03.017.
Li, Z.S., Benchouk, A., Derfouf, F.M., Abou-Bekr, N., Taibi, S., Souli, H. and Fleureau J.M. (2018), "Global representation of the drying-wetting curves of four engineering soils: Experiments and correlations", *Acta Geotech*., **13**(1), 51-71. https://doi.org/10.1007/s11440-017-0527-3.
Liang, J., Huang, R., Prévost, J.H. and Suo, Z. (2003), "Evolving crack patterns in thin films with the extended finite element method", *Int. J. Solids Struct*., **40**, 2343-2354. https://doi.org/10.1016/S0020-7683(03)00095-7.
Liu, D.S. (1965), *The Loess Sedimentation of China,* Science Press, Beijing, China (in Chinese).
Lu, H., Li, J., Wang, W. and Wang, C. (2015), "Cracking and water seepage of Xiashu loess used as landfill cover under wetting–drying cycles", *Environ. Earth Sci*., **74**(11), 7441-7450. https://doi.org/10.1007/s12665-015-4729-4.
Lu, Q., Peng, J., Zhixin, C. and Li, X.A. (2005), "Research on characteristics of cracks and fissures of loess and their distribution in loess plateau of China", *J. Soil Water Conserv*., **19**(5), 191-194 (in Chinese with English abstract).
Mathieu, F., Hild, F. and Roux, S. (2011), "Fatigue crack propagation law measured from integrated digital image correlation: The example of Ti35 thin sheets", *Proc. Eng*., **10**(4), 1091-1096. https://doi.org/10.1016/j.proeng.2011.04.180.
Pan, B., Qian, K., Xie, H. and Asundi, A. (2009), "Two-dimensional digital image correlation for in-plane displacement and strain measurement: a review", *Measmt Sci. Technol.,* **20**(6), 062001. https://doi.org/10.1088/0957-0233/20/6/062001.
Panaghi, K., Golshani, A. and Takemura, T. (2015), "Rock failure assessment based on crack density and anisotropy index variations during triaxial loading tests", *Geomech. Eng*., **9**(6), 793-813. https://doi.org/10.12989/gae.2015.9.6.793.
Park, C.H. and Bobet, A. (2009), "Crack coalescence in specimens with open and closed flaws: A comparison", *Int. J. Rock Mech. Min. Sci*., **46**, 819-829. https://doi.org/10.1016/j.ijrmms.2009.02.006.
Park, C.H. and Bobet, A. (2010), "Crack initiation, propagation

and coalescence from frictional flaws in uniaxial compression", *Eng. Fract. Mech.*, **77**, 2727-2748. https://doi.org/10.1016/j.engfracmech.2010.06.027.

Pasricha, K., Wad, U., Pasricha, R. and Ogale, S. (2009), "Parametric dependence studies on cracking of clay", *Physica A*, **388**, 1352-1358. https://doi.org/10.1016/j.physa.2008.12.039.

Peng, X., Horn, R., Peth, S. and Smucker, A. (2006), "Quantification of soil shrinkage in 2D by digital image processing of soil surface", *Soil Till. Res.*, **91** (1-2), 173-180. https://doi.org/10.1016/j.still.2005.12.012.

Péron, H. (2008), "Desiccation cracking of soils", Ph.D Thesis, Ecole Polytechnique Fédérale de Lausanne, Lausanne, Switzerland.

Péron, H., Hueckel, T., Laloui, L. and Hu, L.B. (2009), "Fundamentals of desiccation cracking of finegrained soils: Experimental characterization and mechanisms identification", *Can. Geotech. J.*, **46**(10), 1177-1201. https://doi.org/10.1139/t09-054.

Reyes, O. and Einstein, H.H. (1991), "Failure mechanisms of fractured rock-a fracture coalescence model", *Proceedings of the 7th International Congress of Rock & Mechanics*, Aachen, Germany, September.

Sagong, M. and Bobet, A. (2002), "Coalescence of multiple flaws in a rock-model material in uniaxial compression", *Int. J. Rock Mech. Min. Sci.*, **39**, 229-241. https://doi.org/10.1016/S1365-1609(02)00027-8.

Shannon, B., Kodikara, J. and Rajeev, P. (2015), "The use of restrained ring test method for soil desiccation studies", *Geotech. Test. J.*, **38**(1), 98-112. https://doi.org/10.1520/GTJ20130131.

Shen, B. and Barton, N. (2018), "Rock fracturing mechanisms around underground openings", *Geomech. Eng.*, **16**(1), 35-47. https://doi.org/10.12989/gae.2018.16.1.035.

Silvestri, V., Sarkis, G., Bekkouche, N. and Soulié, M. (1992), "Evapotranspiration, trees and damage to foundations in sensitive clays", *Proceedings of the Canadian Geotechnical Conference*, Toronto, Canada, October.

Sun, P. (2007), "Experimental research on rupture mechanisms of loess", Ph.D. Dissertation, Chang'an University, Xi'an, China. (in Chinese with English abstract).

Sun, W., Du, H., Zhou, F. and Shao, J. (2019), "Experimental study of crack propagation of rock-like specimens containing conjugate fractures", *Geomech. Eng.*, **17**(4), 323-331. https://doi.org/10.12989/gae.2019.17.4.323.

Sun, X.Z., Shen, B. and Zhang, B.L. (2018), "Experimental study on propagation behavior of three-dimensional cracks influenced by intermediate principal stress", *Geomech. Eng.*, **14**(2), 195-202. https://doi.org/10.12989/gae.2018.14.2.195

Tang, C.A. and Kou, S.Q. (1998), "Crack propagation and coalescence in brittle materials under compression", *Eng. Fract. Mech.*, **61**, 311-324. https://doi.org/10.1016/S0013-7944(98)00067-8.

Tang, C.S., Shi, B., Liu, C., Zhao, L.Z. and Wang, B.J. (2008), "Influencing factors of geometrical structure of surface shrinkage cracks in clayey soils", *Eng. Geol.*, **101**(3-4), 204-217. https://doi.org/10.1016/j.enggeo.2008.05.005.

Tang, C.S., Cui, Y.J., Tang, A.M. and Shi, B. (2010), "Experiment evidence on the temperature dependence of desiccation cracking behavior of clayey soils", *Eng. Geol.*, **114**(3-4), 261-266. https://doi.org/10.1016/j.enggeo.2010.05.003.

Tang, C.S., Shi, B., Liu, C., Suo, W.B. and Gao, L. (2011), "Experimental characterization of shrinkage and desiccation cracking in thin clay layer", *Appl. Clay Sci.*, **52**(1-2), 69-77. https://doi.org/10.1016/j.clay.2011.01.032.

Tay, Y.Y., Stewart, D.I. and Cousens, T.W. (2001), "Shrinkage and desiccation cracking in bentonite - sand landfill liners", *Eng. Geol.*, **60**(1), 263-274. https://doi.org/10.1016/S0013-7952(00)00107-1.

Trabelsi, H., Jamei, M., Zenzri, H. and Olivella, S. (2012), "Crack patterns in clayey soils: Experiments and Modeling", *Int. J. Numer. Anal. Methods Geomech.*, **36**, 1410-1433. https://doi.org/10.1002/nag.1060.

Wang, J. (2000), *Theory and Application of Ground Fissures*, Shaanxi Science and Technology Press, Xi'an, China (in Chinese).

Wang, D.Y., Tang, C.S., Shi, B. and Li, J. (2016), "Studying the effect of drying on soil hydromechanical properties using micro-penetration method", *Environ. Earth Sci.*, **75**(12), 1-13. https://doi.org/10.1007/s12665-016-5836-6.

Wang, L.L., Tang, C.S., Shi, B., Cui, Y.J., Zhang, G.Q. and Hilary I. (2018), "Nucleation and propagation mechanisms of soil desiccation cracks", *Eng. Geol.*, **238**, 27-35. https://doi.org/10.1016/j.enggeo.2018.03.004.

Wei, X. (2014), "Micro-macro study of cracks in clays related to desiccation", Ph.D Dissertation, École Centrale Paris, Châtenay Malabry, France.

Wei, X., Hattab, M. and Fleureau, J.M. (2013), "Micro-macro-experimental study of two clayey materials on drying paths", *B. Eng. Geol. Environ.*, **72**, 495-508. https://doi.org/ 10.1007/s10064-013-0513-4.

Wei, X., Hattab M., Bompard P. and Fleureau, J.M. (2016), "Highlighting some mechanisms of crack formation and propagation in clays on drying path", *Géotechnique,* **66**(4), 287-300. https://doi.org/10.1680/jgeot.14.p.227.

Wei, X., Bicalho, K.V.., Hajjar, A.E., Taibi, S., Hattab, M. and Fleureau, J.M. (2021), "Experimental techniques for the study of the cracking mechanisms in drying clays", *Geotech. Test. J.*, **44**(2), 323-338. https://doi.org/10.1520/GTJ20190430.

Willden, R. and Mabey, D.R. (1961), "Giant desiccation fissures on the black rock and smoke creek deserts, Nevada", *Science,* **133**(3461), 1359-1360. https://doi.org/10.1126/science.133.3461.1359.

Wong, R.H.C., Chau, K.T., Tang, C.A. and Lin, P. (2001), "Analysis of crack coalescence in rock-like materials containing three flaws-Part I: Experimental approach", *Int. J. Rock Mech. Min. Sci.*, **38**, 909-924. https://doi.org/10.1016/S1365-1609(01)00064-8.

Wu, T., Lan, J.W., Qiu, Q.W., He, H.J. and Li, H. (2017), "Behavior and influence of desiccation cracking in loess landfill covers", *IOP Conf. Ser. Earth Environ. Sci.*, **94**(1), 012084. https://doi.org/10.1088/1755-1315/94/1/012084.

Xu, L. and Coop, M. (2016), "Influence of structure on the behavior of a saturated clayey loess", *Can. Geotech. J.,* **53**, 1026-1037. https://doi.org/10.1139/cgj-2015-0200.

Xu, L. and Coop, M. (2017), "The mechanics of a saturated silty loess with a transitional mode", *Géotechnique*, **67**(7), 581-596. https://doi.org/10.1680/jgeot.16.p.128.

Youshida, S. and Adachi, K. (2004), "Numerical analysis of crack generation in saturated deformable soil under row-planted vegetation", *Geoderma*, **120**, 63-74. https://doi.org/10.1016/j.geoderma.2003.08.009.

Zhang, Y., Ye, W.M., Chen, Y.G. and Ye, B. (2016), "Desiccation of NaCl-contaminated soil of earthen heritages in the Site of Yar City, northwest China", *Appl. Clay Sci.*, **124-125**, 1-10. https://doi.org/10.1016/j.clay.2016.01.047.

Zhang, X.D., Chen, Y.G., Ye, W.M., Cui, Y.J., Deng, Y.F. and Chen, B. (2017), "Effect of salt concentration on desiccation cracking behavior of GMZ bentonite", *Environ. Earth Sci.*, **76**, 531. https://doi.org/10.1007/s12665-017-6872-6.

Zhang, T.W., Deng, Y.F., Cui, Y.J., Lan, H.X., Zhang, F.Y. and Zhang, H.Y. (2019), "Porewater salinity effect on flocculation and desiccation cracking behaviour of kaolin and bentonite considering working condition", *Eng. Geol.*, **251**, 11-23. https://doi.org/10.1016/j.enggeo.2019.02.007.

Zhou, X.P., Gu, X.B. and Wang, Y.T. (2015), "Numerical simulations of propagation, bifurcation and coalescence of cracks in rocks", *Int. J. Rock Mech. Min. Sci.*, **80**, 241-254. https://doi.org/10.1016/j.ijrmms.2015.09.006.

Zhou, X.P. and Wang, Y.T. (2016), "Numerical simulation of crack propagation and coalescence in pre-cracked rock-like Brazilian disks using the non-ordinary state-based peridynamics", *Int. J. Rock Mech. Min. Sci.*, **89**, 235-249. https://doi.org/10.1016/j.ijrmms.2016.09.010.

CC